Supplementary Material for: 'Inference of the S- to P-wave velocity anomalies ratio and its uncertainty with an application to South-East Asia'

Emile Serra * [1], Christophe Zaroli [1], Sophie Lambotte [1], and Paula Koelemeijer [2]

[1]Institut Terre et Environnement de Strasbourg, Université de Strasbourg, EOST, CNRS, UMR 7063, 5 rue Descartes, Strasbourg F-67084, France
[2]Department of Earth Sciences, University of Oxford, South Parks Road, OX1 3AN, Oxford, UK

Introduction

In this document, we include further explanations supporting the main body of the article. Are also included figures for our tomographic model SPRUM-Indo spanning over more depths.

Ss1. Hinkley formula

Having two uncorrelated Gaussian distribution $\mathcal{N}_1(\mu_1, \sigma_1^2)$ and $\mathcal{N}_2(\mu_2, \sigma_2^2)$, where $\mu_{1,2}$ and $\sigma_{1,2}$ represent the mean and standard deviation of the two Gaussians. Their division results into the Hinkley distribution, H. This distribution is computed analytically (Hinkley, 1969):

$$
\begin{aligned}
H(w) &\sim \frac{\mathcal{N}_1(\mu_1, \sigma_1^2)}{\mathcal{N}_2(\mu_2, \sigma_2^2)}(w) \\
H(w) &= \frac{b(w)d(w)}{\sqrt{2\pi}\sigma_1\sigma_2 a^3(w)}\operatorname{erf}\left(\frac{b(w)}{a(w)\sqrt{2}}\right) + \frac{\exp\left(-\frac{c}{2}\right)}{\pi\sigma_1\sigma_2 a^2(w)} \\
&\text{with,} \\
a(w) &= \sqrt{\frac{w^2}{\sigma_1^2} + \frac{1}{\sigma_2^2}} \\
b(w) &= \frac{\mu_1}{\sigma_1^2}w + \frac{\mu_2}{\sigma_2^2} \\
c &= \frac{\mu_1^2}{\sigma_1^2} + \frac{\mu_2^2}{\sigma_2^2} \\
d(w) &= \exp\left(\frac{b^2(w) - ca^2(w)}{2a^2(w)}\right),
\end{aligned}
\tag{Se1}
$$

erf is the error function and w indicates an element in the range of values that the division can take.

*Corresponding author: emile.serra@unistra.fr

Ss2. Ratio of absolute velocities

If the Hinkley distribution is not Gaussian due to relative velocity values crossing zero, one might consider analysing the ratio directly using absolute velocity values. However, this approach is not feasible as we demonstrate below.
In the case of error-free data, the velocity perturbation obtained with SOLA is given by:

$$\delta \ln \hat{V}^{(k)} = \int A^{(k)}(r) \delta \ln V(r) d^P r \,, \tag{Se2}$$

where $P = 1,2,3$ represents the dimension, (k) the inquiry point, A the averaging kernel, and $\delta \ln V(r) = \frac{V(r)-V_0(r)}{V_0(r)}$ the true velocity perturbation, which would correspond to either $dlnV_p$ or $dlnV_s$ in the manuscript. V_0 is the reference velocity model (e.g., AK135 in our case). To obtain the SOLA estimate of the absolute velocity, we must compute $\int A^{(k)}(r)\, V(r)\, d^P r$. Thus, equation Se2 can be rewritten as:

$$\delta \ln V^{(k)} = \int A^{(k)}(r) \frac{V(r)-V_0(r)}{V_0(r)} d^P r = \int A^{(k)}(r) \frac{V(r)}{V_0(r)} d^P r - 1 \text{ , (since } \int A = 1), \tag{Se3}$$

which leads to:

$$\int A^{(k)}(r) \frac{V(r)}{V_0(r)} d^P r = 1 + \delta \ln \hat{V}^{(k)} \,. \tag{Se4}$$

This shows that the inverse of the reference model is filtered through the $A^{(k)}$. Thus, $V_0(r)$ can only be factored out of the integral if it is constant over the $A^{(k)}$ volume in all P dimensions. This is feasible in a 2D setup, where the $A^{(k)}$ is constrained to a single depth with a constant value for the 1D reference model, as it would be the case in surface wave tomography. Indeed, when $p = 2$ and $V_0(r) = V_0$, we obtain:

$$\int A^{(k)}(r) V(r) d^2 r = V_0 \left(1 + \delta \ln \hat{V}^{(k)}\right) \,. \tag{Se5}$$

However, in 3D tomography, where $p = 3$ and $V_0(r) \neq V_0$, the reference model is only constant at a fixed depth i. It can generally not be factored and thus it is not possible to compute the absolute velocities with SOLA.

Applying the above to our setup in 3D, we can show that the AK135 model, when viewed through the $A^{(k)}$, differs significantly, by up to $\pm 15\%$ for $dlnV_p$ and $dlnV_s$ compared to the base reference model. This range of variation is far larger than the values seen in our images, making it impossible to revert to absolute values for computing the ratio. That said, SOLA is less biased by the reference model than other inversion methods as we only assume a priori information on the model resolution, not the values.

Ss3. Additional figures for different depths

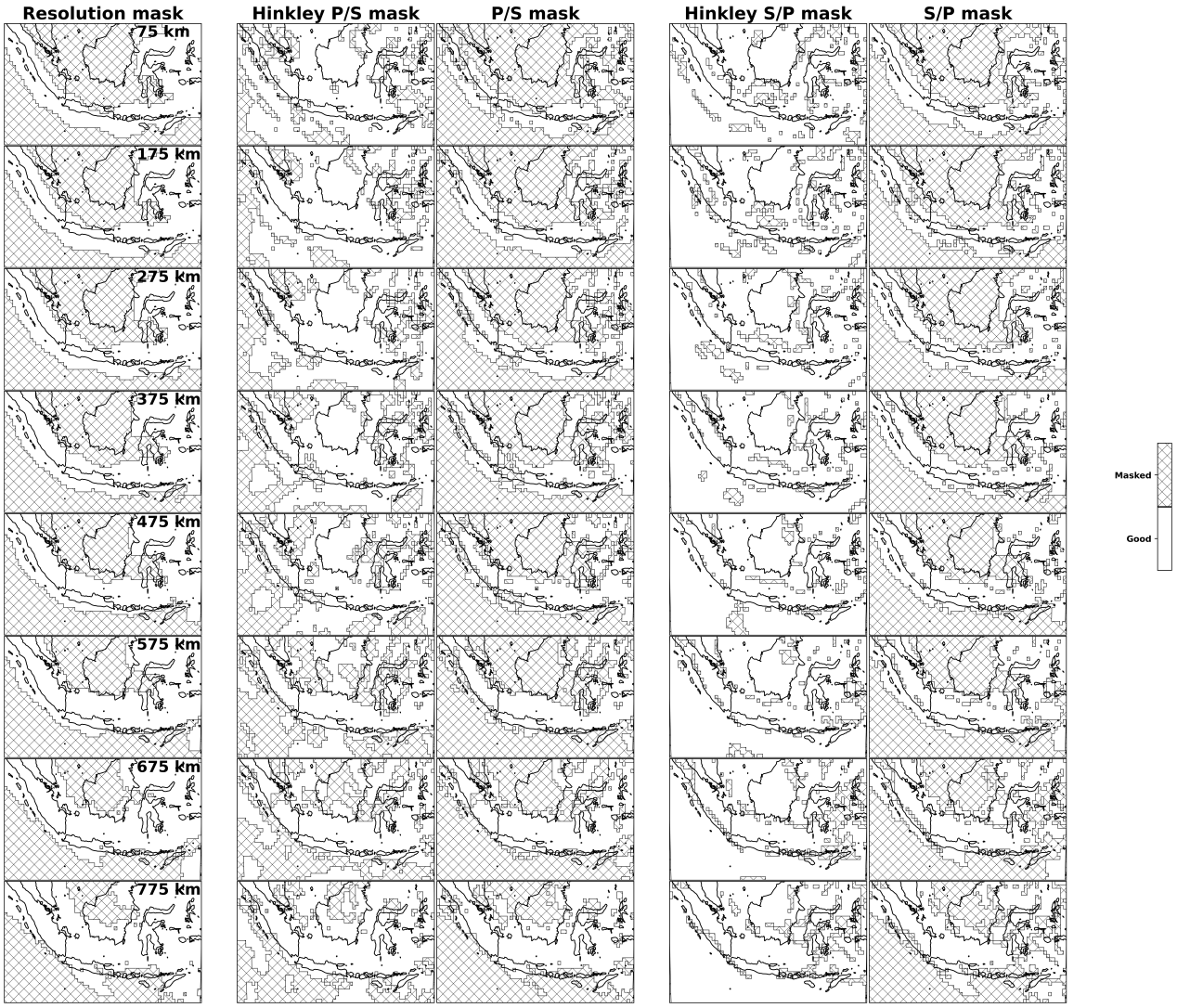

Figure S1: The columns from left to right represent: the resolution mask, the Hinkley mask for the P/S inversion ($1/R = dlnV_p/dlnV_s$), the combination of the two for P/S, the Hinkley mask for the S/P inversion ($R = dlnV_s/dlnV_p$) and its combination with the resolution mask for S/P; for depths of 75 to 775 km, in steps of 100 km from top to bottom

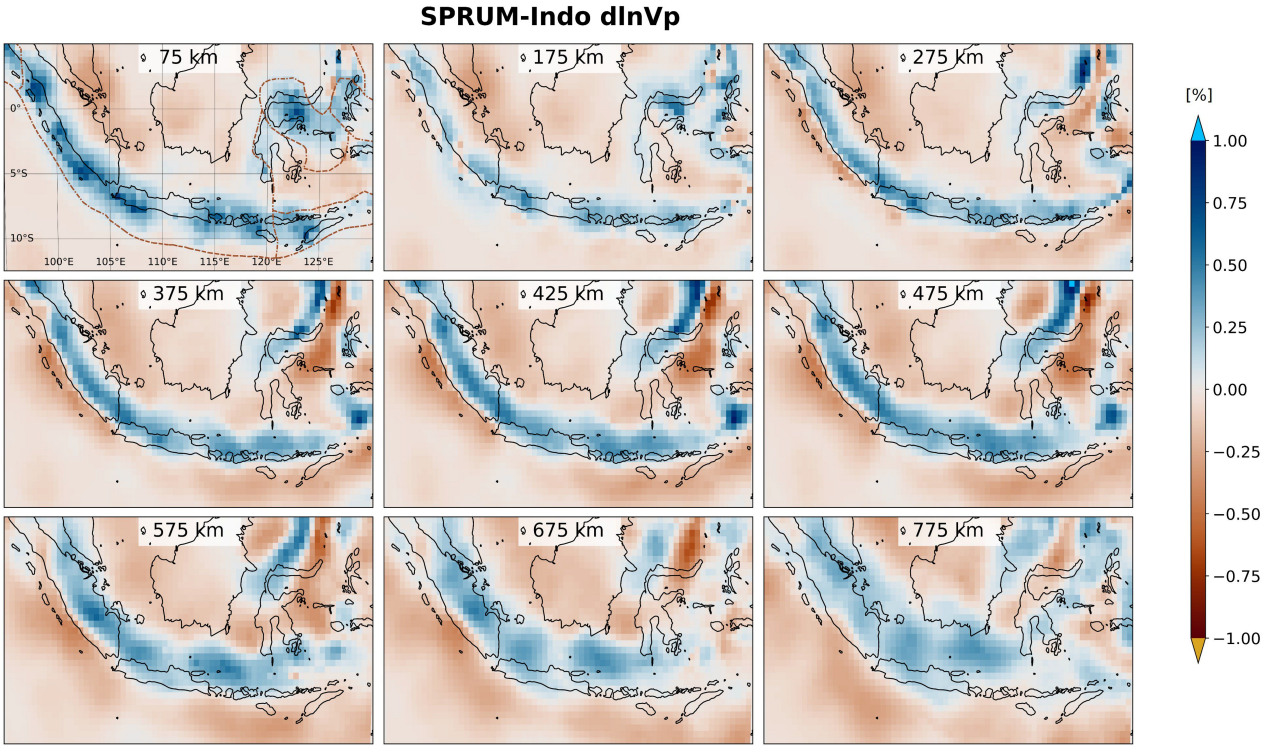

Figure S2: The results of the SOLA inversion for $dlnV_p$ for several depths.

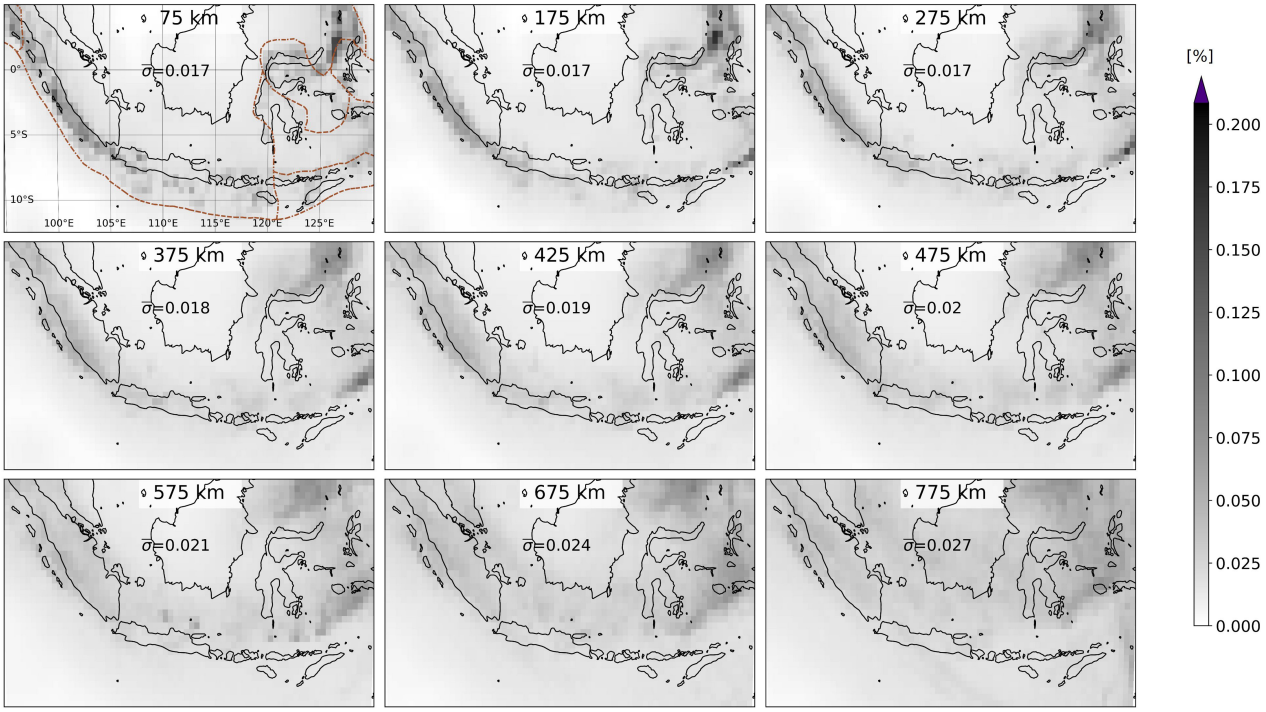

Figure S3: The results of the SOLA inversion for the uncertainty of $dlnV_p$ for several depths. The values of the standard deviation (mean uncertainties of all unmasked cells) are indicated in each map.

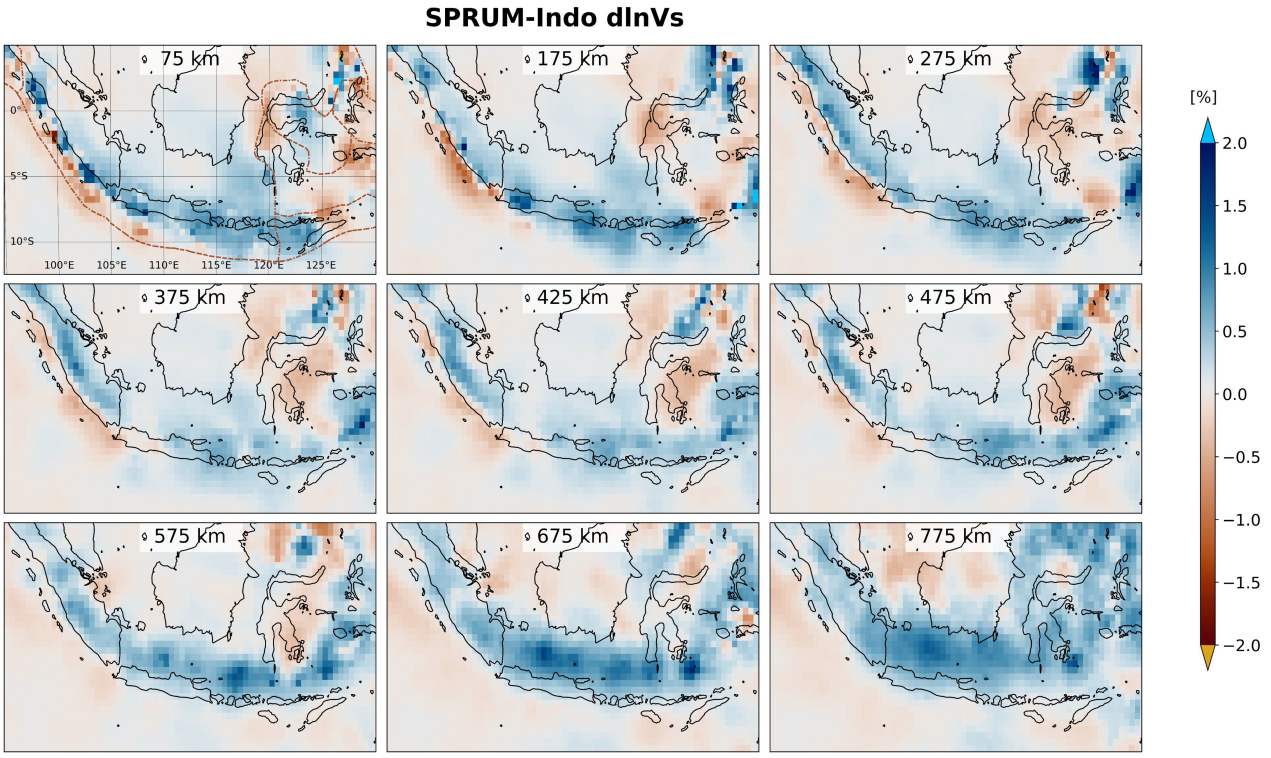

Figure S4: Similar as figure S2, but for $dlnV_s$.

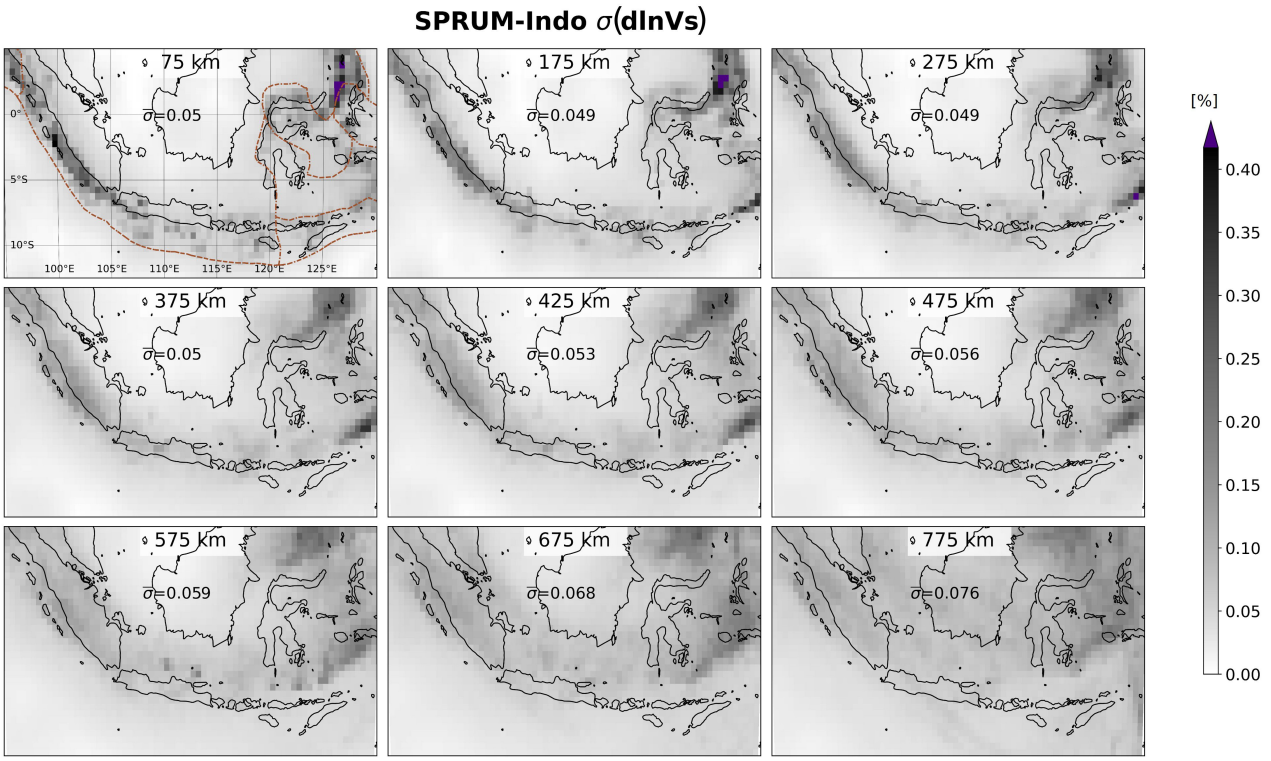

Figure S5: Similar as figure S3, but for the uncertainty of $dlnV_s$.

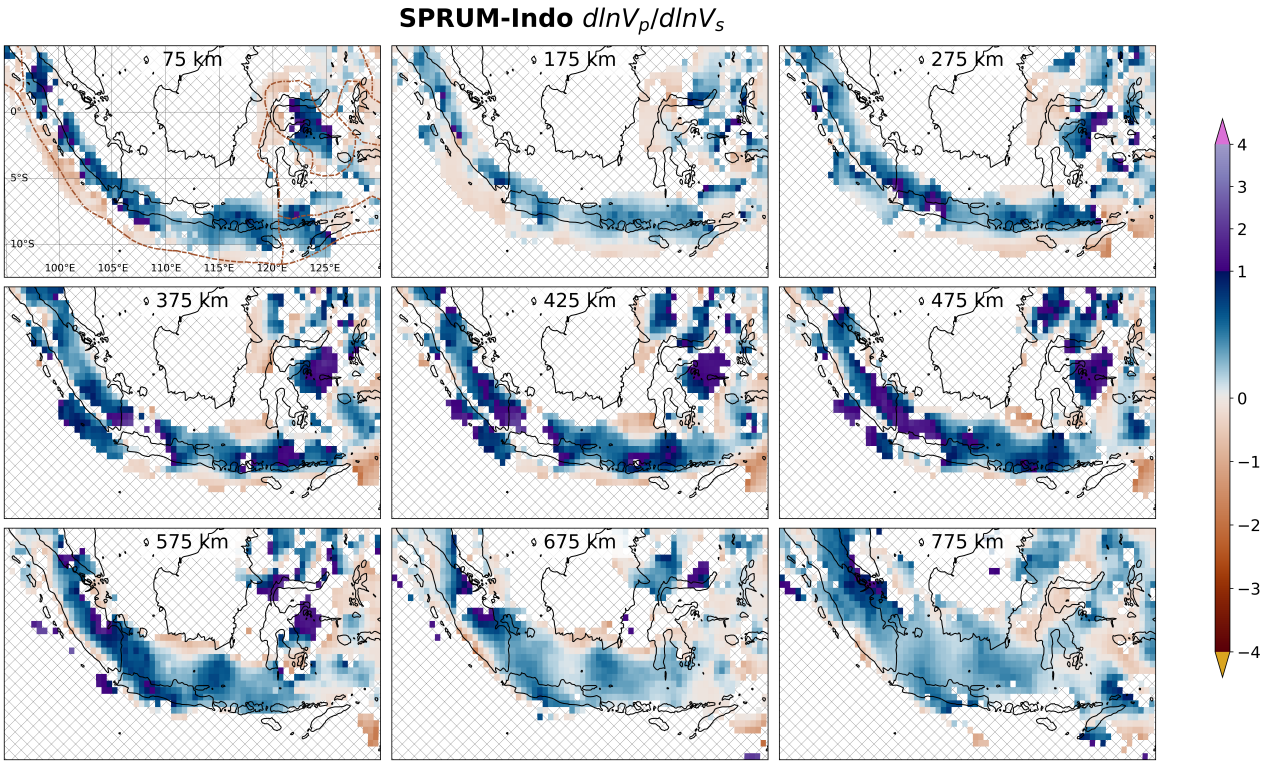

Figure S6: Similar as figure S2, but for $dlnV_p/dlnV_s$.

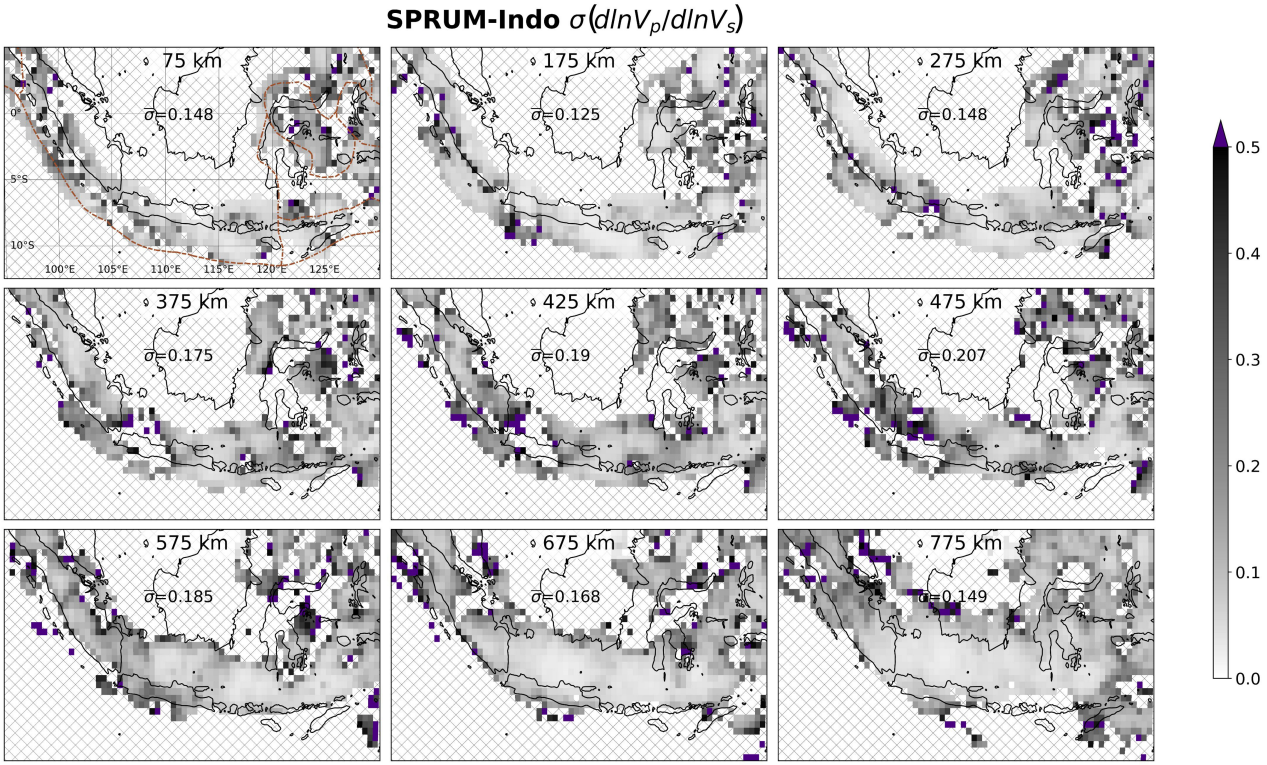

Figure S7: Similar as figure S3, but for the uncertainty of $dlnV_p/dlnV_s$.

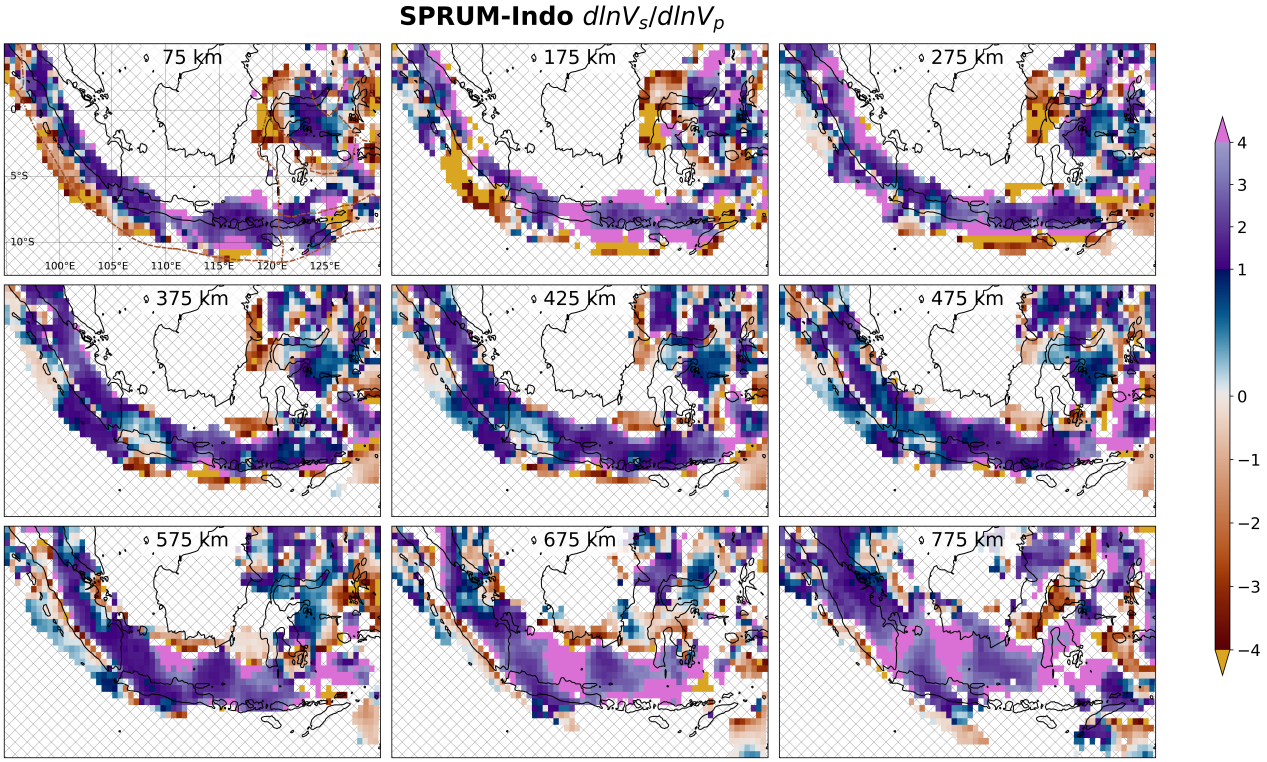

Figure S8: Similar as figure S2, but for $dlnV_s/dlnV_p$.

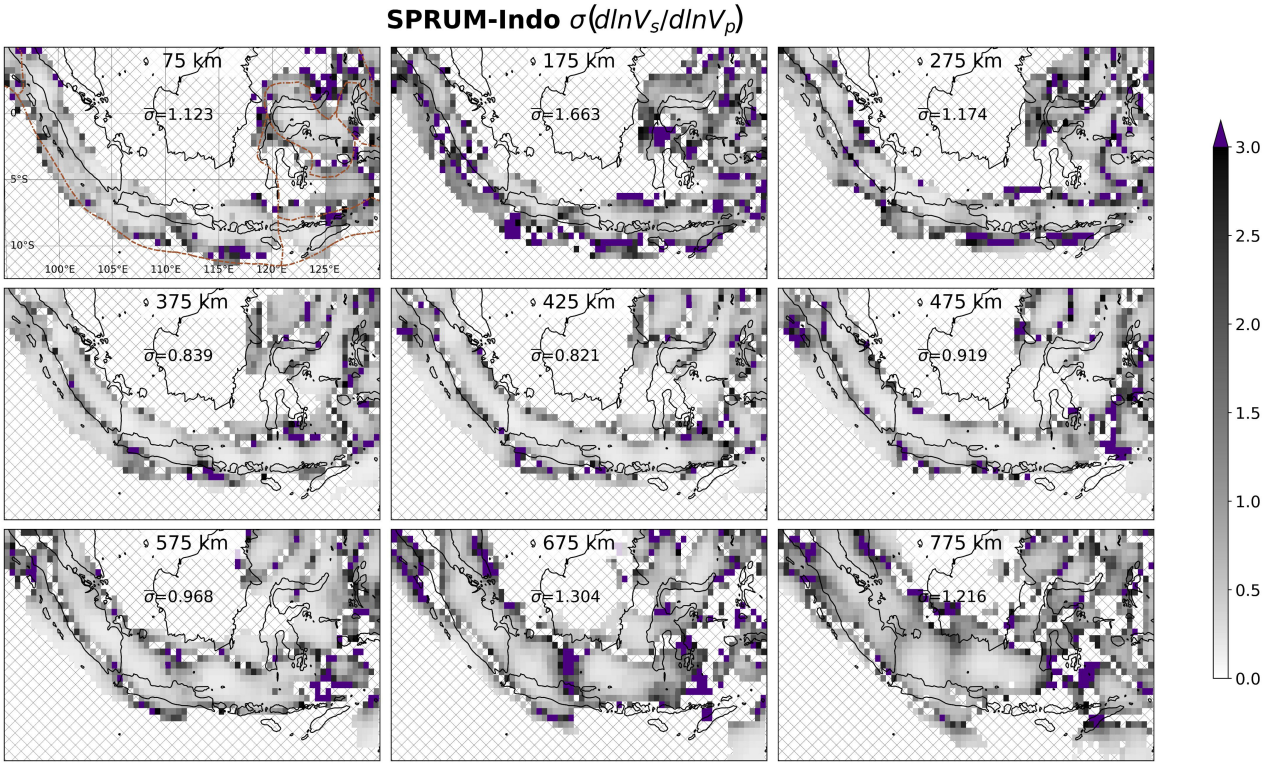

Figure S9: Similar as figure S3, but for the uncertainty of $dlnV_s/dlnV_p$.

S3. Comparisons to existing models

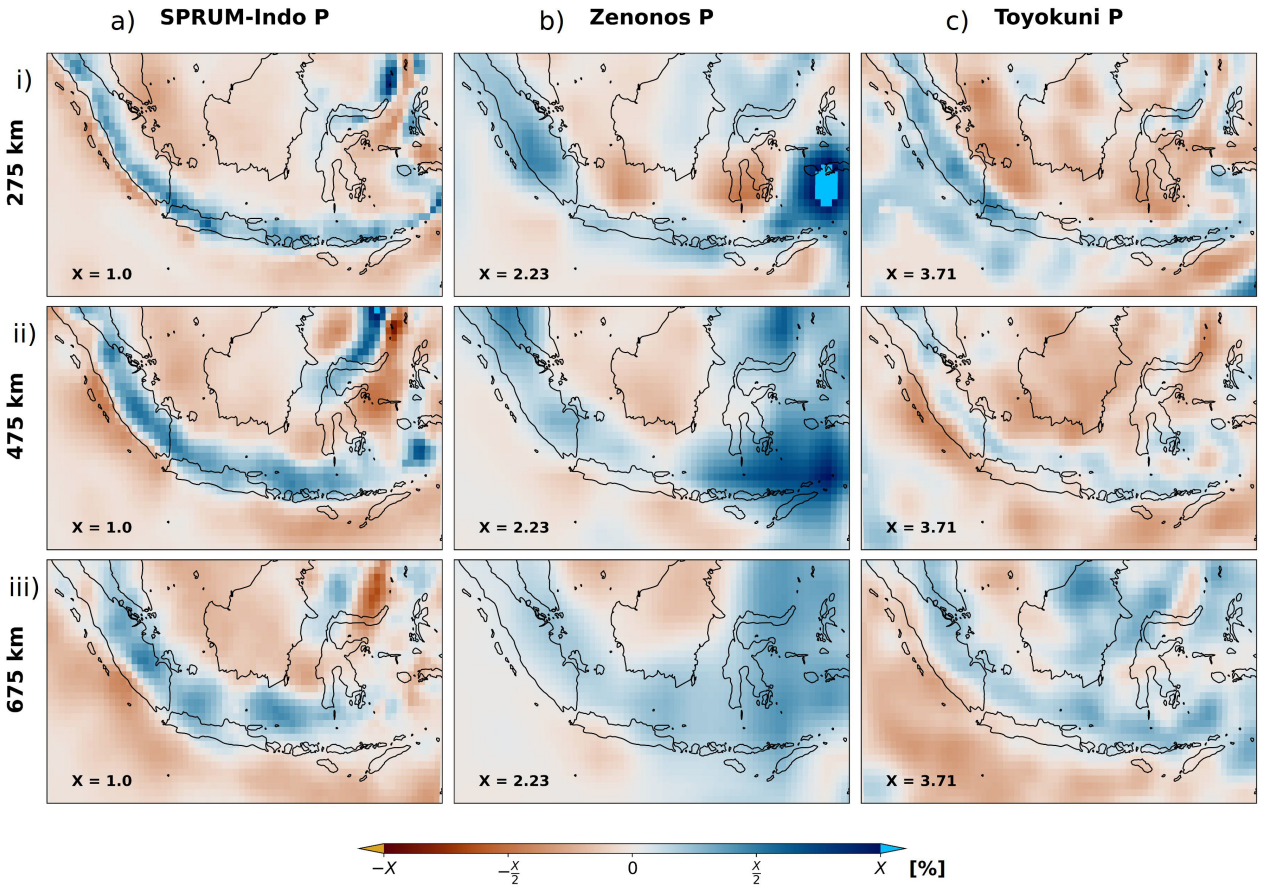

Figure S10: The $dlnV_p$ part of model SPRUM-Indo (a, this study) compared to the $dlnV_p$ models of Zenonos et al. (2019) (b) and Toyokuni et al. (2022) (c), projected on the same tomographic grid, for depths of 275 km (i), 475 km (ii) and 675 km (iii).

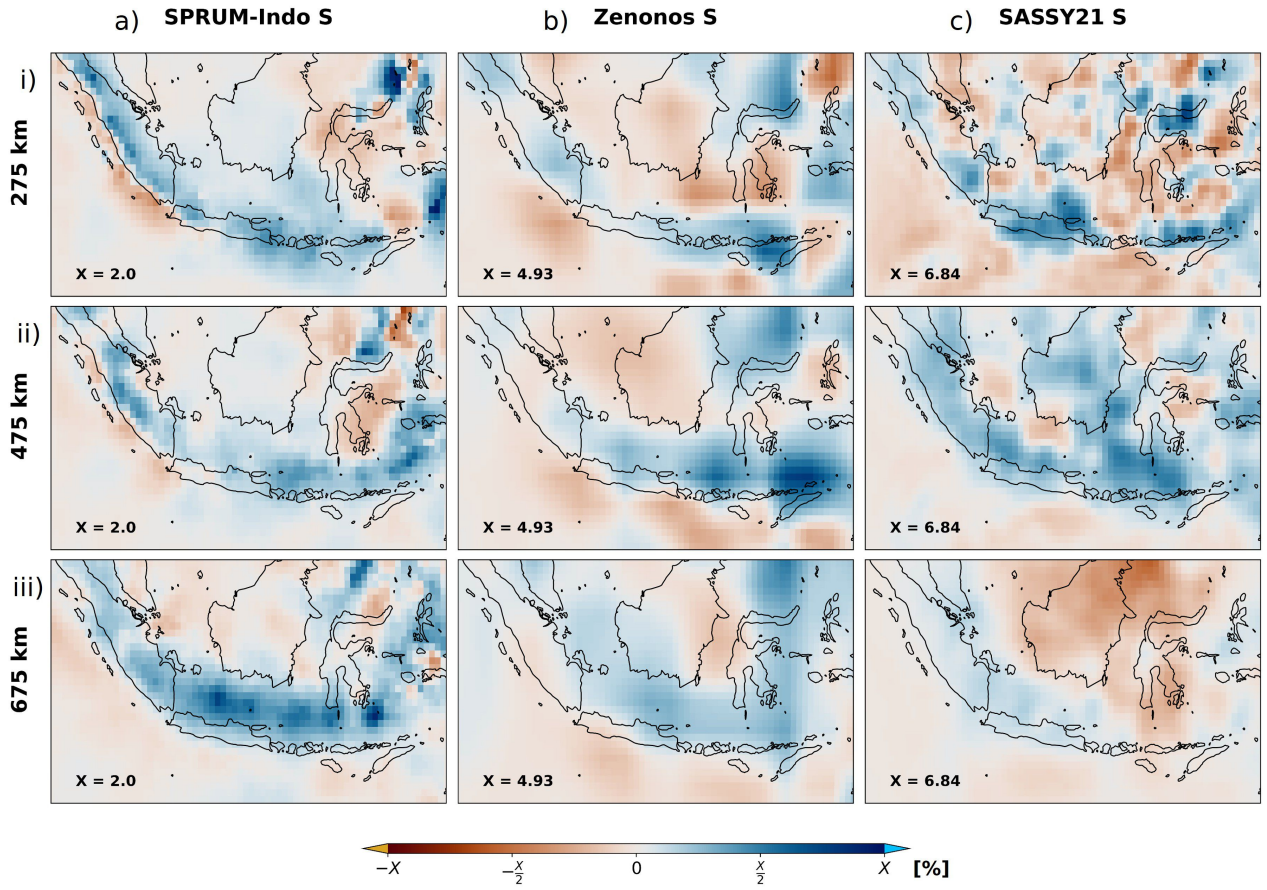

Figure S11: The $dlnV_s$ part of model SPRUM-Indo (a, this study) compared to the $dlnVs$ models of Zenonos et al. (2019) (b) and Wehner et al. (2022) (c), projected on the same tomographic grid, for depths of 275 km (i), 475 km (ii) and 675 km (iii).

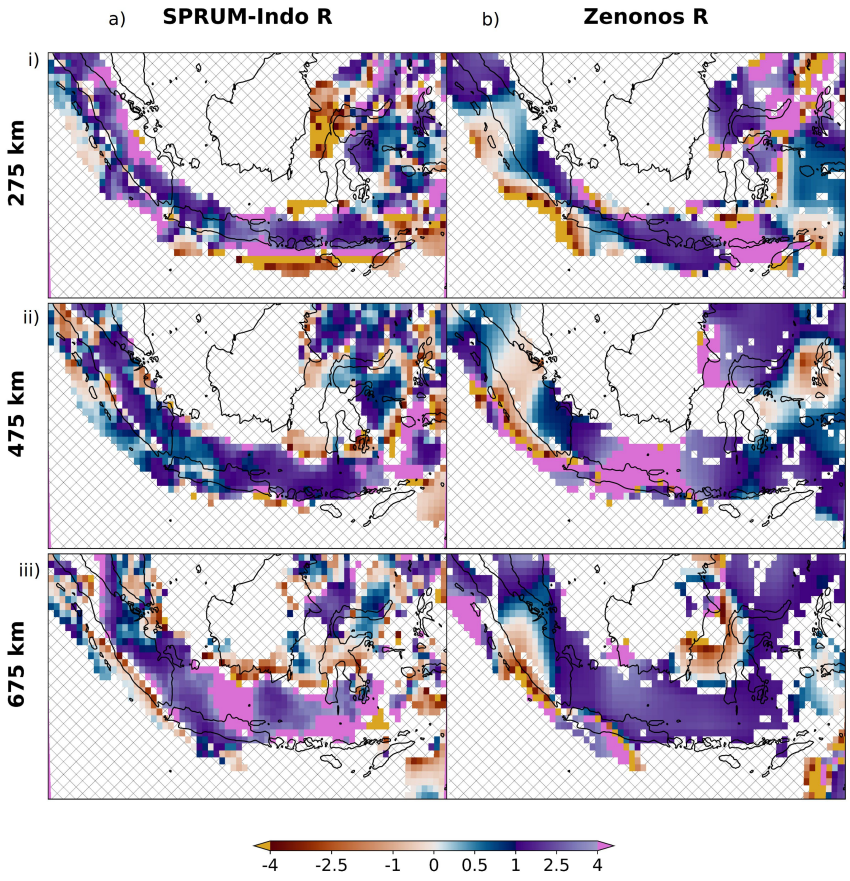

Figure S12: Similar as figure S11, but showing the $dlnV_s/dlnV_p$ model of Zenonos et al. (2020) only. We applied the same mask as computed for our model to the model of Zenonos et al. (2020). As no information on the uncertainties was given by the authors, we simply divided the $dlnV_s$ and $dlnV_p$ values to obtain the R map.

Bibliography

Hinkley, D. V., 1969. On the Ratio of Two Correlated Normal Random Variables, *Biometrika*, **56**(3), 635–639.

Toyokuni, G., Zhao, D., & Kurata, K., 2022. Whole-Mantle Tomography of Southeast Asia: New Insight Into Plumes and Slabs, *Journal of Geophysical Research: Solid Earth*, **127**(11), e2022JB024298, doi: https://doi.org/10.1029/2022JB024298.

Wehner, D., Blom, N., Rawlinson, N., Daryono, Böhm, C., Miller, M. S., Supendi, P., & Widiyantoro, S., 2022. SASSY21: A 3-D Seismic Structural Model of the Lithosphere and Underlying Mantle Beneath Southeast Asia From Multi-Scale Adjoint Waveform Tomography, *Journal of Geophysical Research: Solid Earth*, **127**(3), e2021JB022930, doi: https://doi.org/10.1029/2021JB022930.

Zenonos, A., De Siena, L., Widiyantoro, S., & Rawlinson, N., 2019. P and S wave travel time tomography of the SE Asia-Australia collision zone, *Physics of the Earth and Planetary Interiors*, **293**, 106267, doi: https://doi.org/10.1016/j.pepi.2019.05.010.

Zenonos, A., De Siena, L., Widiyantoro, S., & Rawlinson, N., 2020. Direct Inversion of S-P Differential Arrival Times for Ratio in SE Asia, *Journal of Geophysical Research: Solid Earth*, **125**(5), e2019JB019152, doi: https://doi.org/10.1029/2019JB019152.